Effects of cooling rate on particle rearrangement statistics: Rapidly cooled glasses are more ductile and less reversible

Meng Fan, Minglei Wang, Kai Zhang, Yanhui Liu, Jan Schroers, Mark D. Shattuck, and Corey S. O'Hern

Phys. Rev. E **95**, 022611 — Published 28 February 2017

DOI: 10.1103/PhysRevE.95.022611

The effects of cooling rate on particle rearrangement statistics: Rapidly cooled glasses are more ductile and less reversible

Meng Fan,[1,2] Minglei Wang,[1,2] Kai Zhang,[3] Yanhui Liu,[1,2] Jan Schroers,[1,2] Mark D. Shattuck,[4,1] and Corey S. O'Hern[1,2,5,6]

[1]*Department of Mechanical Engineering and Materials Science, Yale University, New Haven, Connecticut, 06520, USA*
[2]*Center for Research on Interface Structures and Phenomena, Yale University, New Haven, Connecticut, 06520, USA*
[3]*Department of Chemical Engineering, Columbia University, New York, New York 10027, USA*
[4]*Department of Physics and Benjamin Levich Institute, The City College of the City University of New York, New York, New York, 10031, USA*
[5]*Department of Physics, Yale University, New Haven, Connecticut, 06520, USA*
[6]*Department of Applied Physics, Yale University, New Haven, Connecticut, 06520, USA*

(Dated: February 13, 2017)

Amorphous solids, such as metallic, polymeric, and colloidal glasses, display complex spatiotemporal response to applied deformations. In contrast to crystalline solids, during loading, amorphous solids exhibit a smooth crossover from elastic response to plastic flow. In this study, we investigate the mechanical response of binary Lennard-Jones glasses to athermal, quasistatic pure shear as a function of the cooling rate used to prepare them. We find several key results concerning the connection between strain-induced particle rearrangements and mechanical response. We show that the energy loss per strain $dU_{\rm loss}/d\gamma$ caused by particle rearrangements for more rapidly cooled glasses is larger than that for slowly cooled glasses. We also find that the cumulative energy loss $U_{\rm loss}$ can be used to predict the ductility of glasses even in the putative linear regime of stress versus strain. $U_{\rm loss}$ increases (and the ratio of shear to bulk moduli decreases) with increasing cooling rate, indicating enhanced ductility. In addition, we characterized the degree of reversibility of particle motion during a single shear cycle. We find that irreversible particle motion occurs even in the linear regime of stress versus strain. However, slowly cooled glasses, which undergo smaller rearrangements, are more reversible during a single shear cycle than rapidly cooled glasses. Thus, we show that more ductile glasses are also less reversible.

PACS numbers: 62.20.-x, 63.50.Lm 64.70.kj 64.70.pe

I. INTRODUCTION

Amorphous solids, including metallic, polymeric, and colloidal glasses, possess complex mechanical response to applied deformations, such as plastic flow [1–4], strain localization [5–9], creep flow [7, 10, 11], and fracture [12–14]. In crystalline materials, topological defects reflecting the symmetry of the crystalline phase govern response to deformation. In amorphous solids without long-range positional order, it is more difficult to detect and predict changes from elastic response to irreversible behavior [8, 15], such as yielding [16, 17] and flow [4, 18]. The typical response of the deviatoric stress to an applied (pure) shear strain for amorphous solids is depicted in Fig. 1 (a). The average stress increases roughly linearly with strain for small strains, indicating a putative elastic regime. At larger strains, the stress response softens and becomes anelastic, but it continues to increase with strain. For larger strains (*i.e.* near $\gamma \sim 0.05$), the shear stress reaches a peak (whose height depends on the thermal history, as shown in Fig. 1 (c)) and then begins to decrease until it plateaus at a steady state value in the plastic flow regime [2, 18]. (For this system, we employed periodic boundary conditions that prevent fracture.)

Several studies have suggested that amorphous solids do not possess a truly elastic response regime [6, 7, 9, 16, 19–21]. For example, both a sublinear increase of stress versus strain (left inset to Fig. 1 (a)) and rapid drops in stress over narrow strain intervals (right inset to Fig. 1 (a)) have been observed at strains below the nominal yield strain of 2% [16, 19, 21]. The rapid drops in stress are caused by particle rearrangements (Fig. 1 (b)), which are often referred to as shear transformation zones [1, 22–25]. We will show below how the energy loss induced by rearrangements, even in the putative elastic regime, determines the mechanical response of glasses.

In this article, we build a conceptual framework for the thermal history dependent mechanical response of glasses in terms of strain-induced particle rearrangements. Our studies focus on binary Lennard-Jones glasses undergoing athermal, quasistatic pure shear. The initial glasses are prepared over a wide range of cooling rates. The cooling rate determines the fictive temperature, which defines the average energy of the glass in the potential energy landscape [27, 28]. The fictive temperature significantly affects mechanical properties, such as ductility [14, 29, 30], shear band formation [31], and stress versus strain [2, 32]. Prior work has characterized the disappearance of minima in the energy landscape and resulting particle rearrangements versus applied strain [26, 33, 34]. However, how the particle rearrangement statistics contribute to

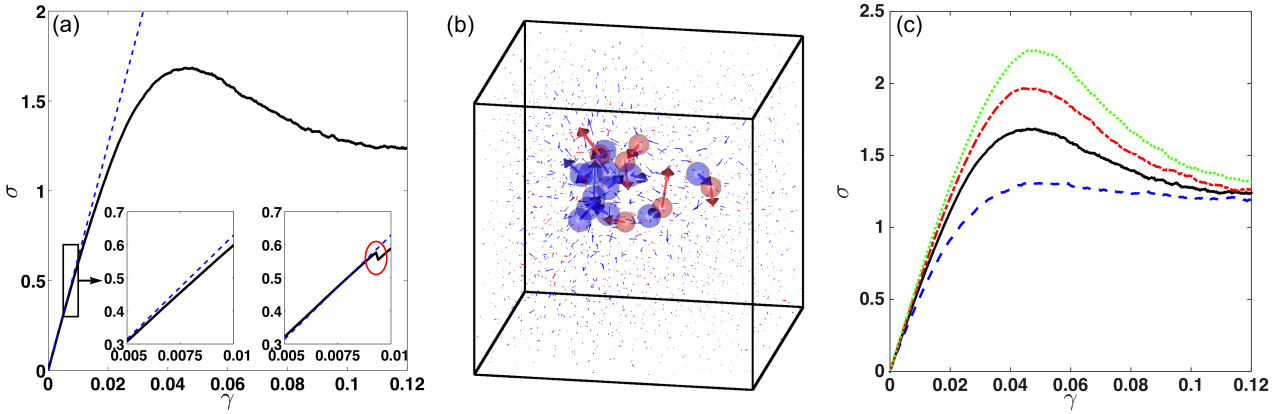

Figure 1: (a) von Mises stress σ versus strain γ (solid line) from simulations of binary Lennard-Jones glasses (prepared at cooling rate $R_c = 10^{-3}$) with $N = 2000$ particles undergoing athermal, quasistatic pure shear averaged over 500 samples. Periodic boundary conditions are employed, which prevent fracture during loading. (The dependence of $\sigma(\gamma)$ on system size is shown in Appendix C.) The affine stress versus strain in the $\gamma \to 0$ limit is given by the dashed line. The left inset provides a close-up of the ensemble-averaged $\sigma(\gamma)$, which highlights the deviation from linear behavior in the range $\gamma = 0.005$ to 0.01. The right inset gives $\sigma(\gamma)$ for a single sample over the same small strain interval. The circled stress drop indicates the particle rearrangement in (b). The vectors (which have been scaled by a factor of 15) indicate the particle displacements that caused the stress drop. The participation number $\mathcal{P}$ [26] of this event is roughly 18. Blue and red spheres indicate the large and small particles, respectively, with the largest displacements. (c) σ versus γ for the same system in (a) for several cooling rates $R_c = 10^{-2}$ (dashed line), 10^{-3} (solid line), 10^{-4} (dash-dotted line), and 10^{-5} (dotted line).

the cooling rate dependent mechanical response is not well understood.

We emphasize three key results concerning the cooling rate dependent mechanical response of glasses. First, we find that the strain-induced energy loss per strain for more rapidly cooled glasses is larger than that for more slowly cooled glasses. Second, we show that the cumulative energy loss before the plastic flow regime can be used to determine whether glasses exhibit brittle or ductile behavior. Third, we characterize the degree of irreversibility of particle rearrangements in response to shear reversal and show that more rapidly cooled glasses are more ductile and irreversible compared to slowly cooled glasses.

II. METHODS

We performed constant number, pressure, and temperature (NPT) molecular dynamics simulations of binary Lennard-Jones mixtures containing 80% large and 20% small spherical particles by number (both with mass m) in a cubic box with volume V under periodic boundary conditions. The particles interact pairwise via the shifted-force version of the Lennard-Jones potential, $u(r_{ij}) = 4\epsilon_{ij}[(\sigma_{ij}/r_{ij})^{12} - (\sigma_{ij}/r_{ij})^{6}]$ with a cutoff distance $r_c = 2.5\sigma_{ij}$, where r_{ij} is the separation between particles i and j. The energy and length parameters are from the Kob-Andersen model: $\epsilon_{AA} = 1.0$, $\epsilon_{BB} = 0.5$, $\epsilon_{AB} = 1.5$, $\sigma_{AA} = 1.0$, $\sigma_{BB} = 0.88$, and $\sigma_{AB} = 0.8$ [35]. Energy, temperature, pressure, and time scales are expressed in units of ϵ_{AA}, ϵ_{AA}/k_B, $\epsilon_{AA}/\sigma_{AA}^3$, and $\sigma_{AA}\sqrt{m/\epsilon_{AA}}$, respectively, where k_B is Boltzmann's constant [36].

We first equilibrate systems in the liquid regime at constant temperature $T_0 = 0.6$ and pressure $P = 0.025$ using a Nosé-Hoover thermostat and barostat, a second-order simplectic integration scheme [37, 38], and time step $\Delta t = 10^{-3}$. We cool systems into a glassy state at zero temperature using a linear cooling ramp, $T(t) = T_0 - R_c t$ over a range of cooling rates from $R_c = 10^{-1}$ to 10^{-6}, all of which are above the critical cooling rate. Thus, all zero-temperature samples are disordered. We apply athermal, quasistatic pure shear at fixed pressure. To do this, we expand the box length and move all particles affinely in the x-direction by a small strain increment $d\gamma_x = d\gamma = 10^{-4}$ and compress the box length and move all particles affinely in the y-direction by the same strain increment $d\gamma_y = -d\gamma$. Following the applied pure shear strain, we minimize the total enthalpy $H = \mathcal{U} + PV$ at fixed pressure $P = 10^{-8}$, where $\mathcal{U} = \sum_{i>j} u(r_{ij})$ is the total potential energy. We successively apply pure strain increments $d\gamma$ and minimize the enthalpy at fixed pressure after each increment to a total strain γ. We studied systems with $N = 250$, 500, 1000, and 2000 particles to assess finite size effects.

We developed a new method to unambiguously determine whether a particle rearrangement occurs with an accuracy on the order of numerical precision, which allows us to detect rearrangements with sizes ranging over more than seven orders of magnitude. To identify particle rearrangements, at each strain γ we compare the potential energy per particle $U(\gamma) = \mathcal{U}(\gamma)/N$ during forward shear to $U'(\gamma)$ obtained by first a forward shear step from strain γ to $\gamma + d\gamma$ (and enthalpy minimization) followed by a

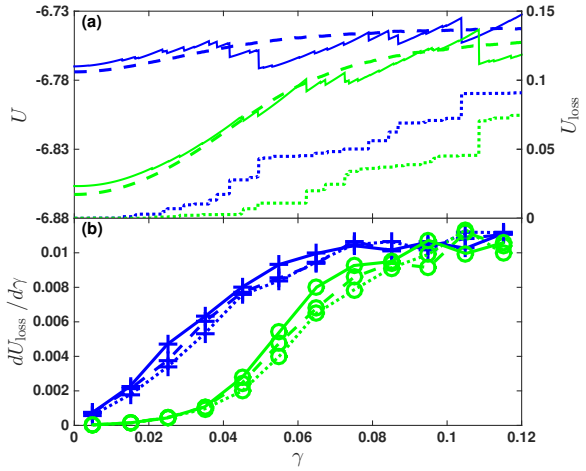

Figure 2: (a) Potential energy per particle $U(\gamma)$ versus strain γ for binary Lennard-Jones glasses with $N = 2000$ particles prepared using cooling rates $R_c = 10^{-2}$ (blue) and 10^{-5} (green) and subjected to athermal, quasistatic pure shear. The solid and dashed lines indicate $U(\gamma)$ for single configurations and averaged over an ensemble of configurations, respectively. The dotted lines indicate the cumulative energy loss up to strain γ, $U_{\rm loss}(\gamma)$, for single configurations. (b) Average energy loss per (1%) strain $dU_{\rm loss}/d\gamma$ versus strain for $R_c = 10^{-2}$ (plus signs) and 10^{-5} (circles) and three system sizes: $N = 2000$ (solid lines), 1000 (dashed lines), and 500 (dotted lines). Ensemble-averaged data is averaged over at least 500 samples.

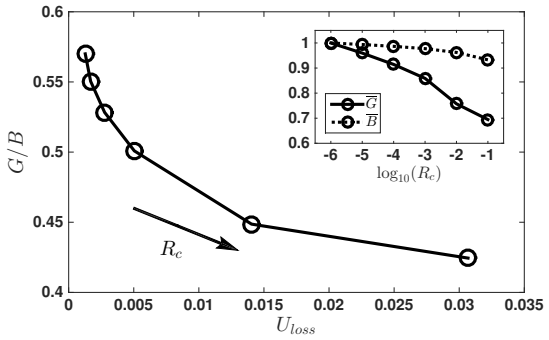

Figure 3: Ratio of shear to bulk moduli G/B versus the cumulative energy loss $U_{\rm loss}$ during shear from $\gamma = 0$ to 0.04 below the peaks in stress versus strain (Fig. 2 (c)). The arrow indicates the direction of increasing R_c. The inset shows $\overline{G}$ and $\overline{B}$ separately versus R_c, both of which are normalized to 1 at $R_c = 10^{-6}$.

backward shear step from $\gamma + d\gamma$ back to γ (and enthalpy minimization). We find that the distribution of magnitudes of the energy differences $|\Delta U(\gamma)| = |U(\gamma) - U'(\gamma)|$ is bimodal with peaks near 10^{-14} corresponding to numerical error and 10^{-3} corresponding to distinct particle rearrangements. Thus, it is straightforward to identify particle rearrangements as those with $|\Delta U| > U_t$, where the threshold $U_t = 10^{-10}$ clearly distinguishes numerical error from particle rearrangements. (See Appendix B for an expanded description of this method.) We denote the total number of rearrangements in the strain interval 0 to γ as $N_r(\gamma)$. In addition, we calculate the energy lost after the $N_r(\gamma)$ rearrangements in the strain interval 0 to γ: $U_{\rm loss}(\gamma) = \sum_{i=1}^{N_r(\gamma)} |\Delta U(\gamma_i)|$, where γ_i indicates strains at which rearrangements occur. For each cooling rate R_c, we detect rearrangements of glasses all prepared at R_c and average $U_{\rm loss}$ over at least 500 samples. Additional details concerning the simulation methods are included in Appendix A.

III. RESULTS

In Fig. 2 (a), we plot $U(\gamma)$ for single configurations, as well the ensemble-averaged curves, for two cooling rates ($R_c = 10^{-5}$ and 10^{-2}). In addition, we show $U_{\rm loss}(\gamma)$ for single configurations at the two cooling rates. The energy loss grows more rapidly at small strains and is thus larger for more rapidly cooled glass. This behavior is consistent with the dependence of $\sigma(\gamma)$ on cooling rate in Fig. 1 (c). As the cooling rate decreases, the yield stress and strain increase because fewer and smaller particle rearrangements occur. However, at large strains, beyond the yield strain, $\sigma(\gamma)$, as well as $U(\gamma)$, become independent of cooling rate [2, 32].

Previous studies have shown that the number of energy minima grows exponentially with the average potential energy [28, 39]. The increase in the number of minima for rapidly cooled glasses makes them more susceptible to particle rearrangements and increased energy loss [40, 41]. Researchers have also shown that more rapidly cooled glasses are more loosely packed and less ordered than slowly cooled glasses [42, 43]. (See results for the packing density versus strain for several cooling rates in Appendix D.) More loosely packed glasses with reduced short- to medium-range structural order are more prone to particle rearrangements and energy loss during shear [16].

In Fig. 2 (b), we plot the ensemble-averaged cumulative energy loss per strain $dU_{\rm loss}/d\gamma$ versus strain. For rapidly cooled glasses, the energy loss is roughly proportional to strain for $\gamma < 0.06$. In contrast, for more slowly cooled glasses (*i.e.* $R = 10^{-5}$), the systems only begin losing energy beyond a characteristic strain $\gamma_c \approx 0.02$. At large strains $\gamma \gtrsim 0.09$, $dU_{\rm loss}/d\gamma$ becomes independent of cooling rate and strain [32]. Further, we find that $dU_{\rm loss}/d\gamma$ is roughly independent of system size over the range of N we consider.

We next connect particle rearrangements to the mechanical properties of glasses. As shown in Fig. 2, more rapidly cooled glasses suffer larger energy loss during shear. We propose that enhanced energy loss through particle rearrangements at small strains can prevent catastrophic brittle failure, by preventing stress accumulation and localization [29, 31, 41, 44, 45]. This suggests that more rapidly cooled glasses are more ductile than

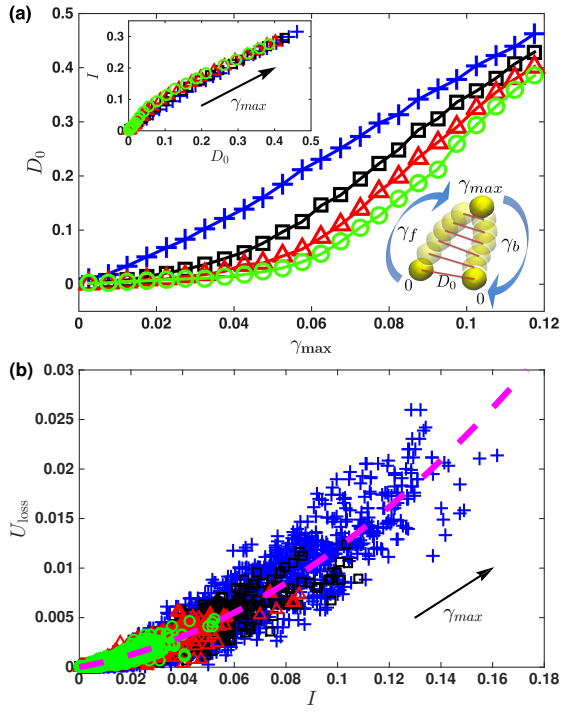

Figure 4: (a) Measure of state irreversibility D_0 after undergoing a single athermal quasistatic pure shear cycle with strain amplitude $\gamma_{\max}$ for several cooling rates: $R_c = 10^{-2}$ (plus signs), 10^{-3} (squares), 10^{-4} (triangles), and 10^{-5} (circles). The curves were averaged over 96 samples with $N = 2000$. The upper left inset shows that the two measures of irreversibility, D_0 and I, are positively correlated. The lower right inset shows a schematic of the trajectory of a single particle during forward shear from total strain 0 to $\gamma_{\max}$ and backward shear from $\gamma_{\max}$ to 0. The bars connect particle positions at corresponding strains during the trajectory, $\vec{R}(\gamma', 0)$ and $\vec{R}(\gamma_{max}, \gamma_{max} - \gamma')$. D_0 and I are related to the length of the lower bar and average length over all bars, respectively. (b) Cumulative energy loss $U_{\rm loss}(\gamma_{max})$ versus path irreversibility $I(\gamma_{max})$ for $0 < \gamma_{max} < 0.04$. Each data points represent a shear cycle with $\gamma_{max} = \gamma_i$, where γ_i are the strains at which rearrangements occur. The dashed curve gives $U_{\rm loss} = \mathcal{A} I^2$ with $\mathcal{A} \sim 1$. The arrow indicates the direction of increasing γ_{max}.

slowly cooled glasses [14].

To investigate this hypothesis, we calculate the cumulative energy loss $U_{\rm loss}$ due to particle rearrangements (from $\gamma = 0$ to 0.04 below the peaks in $\sigma(\gamma)$ as shown in Fig. 2 (c)) as a function of the ratio of the shear to bulk moduli G/B, which correlates strongly with the ductility of a material [14, 44, 46, 47]. (G and B were obtained from the slope of the corresponding stress versus strain for vanishingly small pure and compressive strains, respectively.) As shown in Fig. 3, the brittleness G/B decreases as $U_{\rm loss}$ increases. Moreover, we find that both G and B decrease with increasing cooling rate, but G decreases faster (inset to Fig. 3), and thus the ratio G/B, and brittleness, decrease with increasing R_c.

Whether a material is reversible or not during deformation is often inferred from the stress-strain curve or other macroscopic measurements. For example, materials are typically deemed reversible in the regime where the stress-strain curve is linear, and irreversible in the regime where plastic flow occurs [48]. Reversibility has been studied experimentally using enthalpy [18] and strain recovery [19], elastostatic compression [16], nanoindentation [10], and quality factor measurements [49]. In simulations, reversibility has been studied using cyclic shear of model glasses [17, 50–54]. Though the linear stress-strain region in Fig. 1 is typically considered reversible, recent measurements have identified irreversible events and anelasticity on the micro-scale in this 'elastic' region [6, 7, 9, 16, 19–21].

An important, open challenge is to determine the onset [50, 51] of micro-scale irreversibility and understand its connection to irreversibility and plasticity on macroscopic scales. Above, we defined particle rearrangements as those that led to local irreversibility of the potential energy (quantified by $|\Delta U(\gamma)|$) after a forward strain increment $d\gamma$, followed by a backward strain increment $-d\gamma$. We now characterize reversibility following a single cycle of a *finite-sized* strain using two measures [50]. First, we define "state" irreversibility as

$$D_0(\gamma) = |\vec{R}(0,0) - \vec{R}(\gamma,\gamma)|/N, \qquad (1)$$

where $\vec{R}(\gamma_f, \gamma_b)$ gives the particle coordinates after the system has been sheared forward by strain γ_f and backward by strain γ_b. D_0 characterizes the ability of a sheared system to return to the original, unsheared configuration after a single cycle. (See lower right inset to Fig. 4 (a).) In Eq. 1, $\vec{R}(0,0)$ gives the original, unsheared particle coordinates, and $\vec{R}(\gamma,\gamma)$ gives the particle coordinates of the system after it was sheared forward to strain γ and then sheared backward from γ to 0. $D_0(\gamma) \sim 0$ indicates a type of reversible behavior, where most of the particles return to their original, unsheared positions after a single strain cycle of amplitude γ. In contrast, $D_0 > 0$ implies irreversible behavior that grows in magnitude with increasing D_0. We also define a measure of "path" irreversibility [50],

$$I(\gamma) = \frac{1}{N}\sqrt{\frac{1}{\gamma}\int_0^{\gamma} |\vec{R}(\gamma',0) - \vec{R}(\gamma,\gamma-\gamma')|^2 d\gamma'}, \qquad (2)$$

which gives the average distance between configurations at corresponding strains during forward and backward portions of the shear cycle. (See the lower right inset to Fig. 4 (a).)

Even though shear cycles can occur with $I > 0$ and $D_0 = 0$, which implies that the system returns to the original, unsheared configuration at $\gamma = 0$ along different forward and backward shear paths [50], we find that the ensemble-averaged I becomes nonzero only when D_0 begins increasing from zero. Further, I and D_0 are strongly correlated as $\gamma_{\max}$ increases. (See the upper left inset in Fig. 4 (a).) In Fig. 4 (a), we plot $D_0(\gamma_{max})$ for several

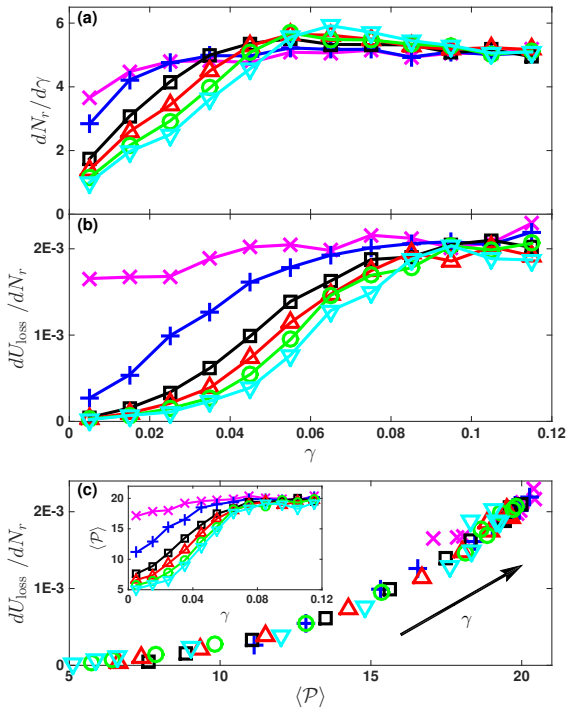

Figure 5: (a) Rearrangement frequency $dN_r/d\gamma$ and (b) energy loss per rearrangement $dU_{\rm loss}/dN_r$ plotted versus strain γ for $R_c = 10^{-1}$ (crosses), 10^{-2} (plus signs), 10^{-3} (squares), 10^{-4} (upward triangles), 10^{-5} (circles), and 10^{-6} (downward triangles). (c) Energy loss per rearrangement $dU_{\rm loss}/dN_r$ plotted parametrically against participation number $\langle\mathcal{P}\rangle$ for all data in (a) and (b). The inset shows $\langle\mathcal{P}\rangle$ versus γ for the same R_c in (a) and (b). All data is obtained by averaging over 500 samples for $N = 2000$.

R_c. We find that slowly cooled glasses are nearly state reversible over a finite range of strain (up to $\gamma_{\rm max} \sim 0.05$), while $D_0 \sim A\gamma_{\rm max}$ (with slope A) for rapidly cooled glasses. For intermediate R_c, $D_0 \sim B(R_c)\gamma_{\rm max}$ for $\gamma_{\rm max} < \gamma_c(R_c)$ and $D_0 \sim A\gamma_{\rm max}$ for $\gamma_{\rm max} > \gamma_c(R_c)$. The slope $B(R_c)$ increases with R_c, and the crossover strain $\gamma_c(R_c)$ decreases with R_c. The upper inset to Fig. 4 (a) shows that I and D_0 possess the same R_c dependence. Rapidly cooled glasses possess higher values of irreversibility because the energy loss during shear is larger (Fig. 2). Further evidence for this is provided in Fig. 4 (b), where we show that $U_{\rm loss} \sim I^2$.

IV. CONCLUSIONS AND FUTURE DIRECTIONS

In this study, we showed that the energy loss per strain $dU_{\rm loss}/d\gamma$ is larger for more rapidly cooled glasses. Further, we found that the cumulative energy loss can be used to determine the ductility and degree of irreversibility of glasses. A future direction of this research is to understand the separate contributions of the frequency of rearrangements $dN_r/d\gamma$ and energy loss per rearrangement $dU_{\rm loss}/dN_r$ to $dU_{\rm loss}/d\gamma = (dU_{\rm loss}/dN_r)(dN_r/d\gamma)$. In Fig. 5 (a) and (b), we show that both $dN_r/d\gamma$ and $dU_{\rm loss}/dN_r$ are larger for more rapidly cooled glasses at small strains. However, in the range $0.05 \lesssim \gamma \lesssim 0.09$, $dN_r/d\gamma$ forms a small peak for small R_c (increasing above the value for large R_c) before reaching the cooling rate independent, large strain limit. The increase in $dN_r/d\gamma$ at intermediate strains is associated with the fact that more slowly cooled glasses develop a large stress overshoot in this regime, as shown in Fig. 1 (c) [2, 31]. In contrast, $dU_{\rm loss}/dN_r$ monotonically increases with γ for all R_c studied.

We find that the energy loss per rearrangement is controlled by the number of particles that move significantly during each rearrangement, which can be quantified using the participation number $\mathcal{P} = \sum_{i=1}^{N} (d_i/d_{max})^2$, where d_i is the displacement of particle i and d_{max} is the maximum d_i [26]. In the inset of Fig. 5 (c), we show that the ensemble-averaged $\langle\mathcal{P}\rangle$ increases with γ and is larger for more rapidly cooled glasses. In contrast, rearrangements are more localized for slowly cooled glasses. We also find that the R_c dependence of $dU_{\rm loss}/dN_r$ can be collapsed when $dU_{\rm loss}/dN_r$ is plotted versus $\langle\mathcal{P}\rangle$, which further emphasizes that the number of particles that move significantly determines energy loss from rearrangements.

An important topic of future research is to characterize the system size dependence of $dN_r/d\gamma$ and $dU_{\rm loss}/d\gamma$, separately, as a function of strain γ. Previous studies [55–57] have shown that the rearrangement frequency displays power-law scaling with system size, $dN_r/d\gamma \sim N^{-\beta}$, with an exponent β whose magnitude varies strongly as the strain is increased above the yielding transition. Beyond yielding in the steady state regime, β reaches a plateau value that is insensitive to cooling rate [55], similar to the behavior for $\sigma(\gamma)$ and $dU_{\rm loss}/d\gamma$. In contrast, the system size dependence of $dU_{\rm loss}/d\gamma$ over the full range of strain is not well-studied, and will be characterized in future studies. The goal of our research in this area is to use the statistics of rearrangements (*i.e.* frequency and energy loss per rearrangement) to build a quantitatively accurate theoretical framework for the cooling-rate dependent mechanical response of glasses.

Acknowledgments

The authors acknowledge primary financial support from NSF MRSEC DMR-1119826 (K.Z.) and partial support from NSF Grant Nos. CMMI-1462439 (C.O. and M.F.) and CMMI-1463455 (M.S.). This work also benefited from the facilities and staff of the Yale University Faculty of Arts and Sciences High Performance Computing Center and the NSF (Grant No. CNS-0821132) that, in part, funded acquisition of the computational facilities.

Appendix A: Athermal, quasistatic pure shear at fixed pressure

In this appendix, we provide additional details concerning the preparation and shearing of zero-temperature glasses. We prepared zero-temperature glasses by cooling the systems from an initial temperature $T_0 = 0.6$ in the liquid regime to zero temperature at fixed pressure $P = 0.025$ using a linear cooling ramp. In this case, the temperature as a function of time t obeys $T(t) = T_0 - R_c t$ with cooling rate R_c. We then minimized the enthalpy $H = \mathcal{U} + PV$, where $\mathcal{U}$ is the total potential energy and $V = L_x L_y L_z$ is the volume, to set the pressure $P_0 = 10^{-8}$ by moving the particles and adjusting the length of the box L_z in the z-direction (by less than 0.1%). We then applied athermal, quasistatic pure shear at fixed low pressure $P_0 = 10^{-8}$ to the zero-temperature glasses. To implement pure shear, we expand the box by a small strain increment $d\gamma_x = \ln(1 + \Delta L_x/L_x) = d\gamma = 10^{-4}$ and move all particles affinely in the x-direction by the same amount. At the same time, we compress the box by a small strain increment $d\gamma_y = \ln(1 - \Delta L_y/L_y) = -d\gamma$ and move all particles affinely in the y-direction by the same amount. After each strain step, we minimize the enthalpy at fixed P_0, by first moving the particles to minimize H at fixed V and then by shifting the particles affinely, and change L_z to set $P = P_0$. After each strain step, the minimization procedure terminates when the magnitude of force on each particle falls below a small tolerance, $f_{\rm max} < f_{\rm tol} = 10^{-10}$, *and* the deviation in the calculated pressure from the target value is small, $|P - P_0|/P_0 < 10^{-4}$.

Appendix B: Identification of particle rearrangements

In many prior studies, somewhat arbitrary thresholds in either energy or nonaffine displacements have been employed to identify particle rearrangement events during athermal, quasistatic shear [1, 8, 52]. In this study, we developed a novel particle rearrangement detection method that identifies particle rearrangements with accuracies that approach numerical precision. To identify particle rearrangements, at each strain γ we compare the total potential energy per particle $U(\gamma) = \mathcal{U}(\gamma)/N$ from simulations undergoing forward shear to the potential energy per particle $U'(\gamma)$ obtained by first a forward shear step from strain γ to $\gamma + d\gamma$ (and enthalpy minimization) followed by a backward shear step from $\gamma + d\gamma$ back to γ (and enthalpy minimization). (See the inset to Fig. 6 (b).) We find that $P(|\Delta U(\gamma)|)$ is bimodal with strong peaks near 10^{-14} corresponding to numerical error and 10^{-3} corresponding to distinct particle rearrangements (Fig. 6 (a)).

We also quantified rearrangements by calculating the non-affine displacement per particle $\mathcal{D}(\gamma)$ between the configurations at successive strain steps γ and $\gamma + d\gamma$ [1]:

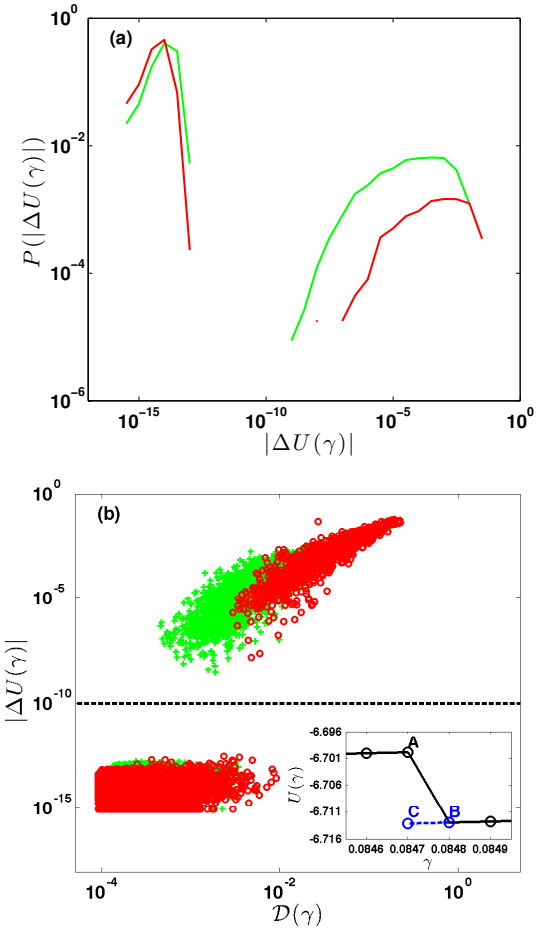

Figure 6: (a) Probability distribution $P(|\Delta U(\gamma)|)$ of the magnitude of the potential energy difference during forward and backward shear $|\Delta U(\gamma)| = |U(\gamma) - U'(\gamma)|$ on a $\log_{10} - \log_{10}$ scale for each strain step during athermal, quasistatic pure shear of binary Lennard-Jones glasses from 96 samples prepared with cooling rate $R_c = 10^{-5}$ and system sizes $N = 250$ (red curves) and 2000 (green curves). (b) A scatter plot of $|\Delta U(\gamma)|$ and the non-affine displacement $\mathcal{D}(\gamma)$ for system sizes $N = 250$ (red circles) and 2000 (green crosses). The horizontal dashed line indicates an unambiguous threshold $U_t = 10^{-10}$ that separates numerical noise (bottom) from particle rearrangements (top). The inset shows the potential energy per particle U versus strain γ for forward and backward shear on a single sample with $N = 250$ that undergoes a particle rearrangement. The black solid line indicates forward shear in increments of $d\gamma = 10^{-4}$, *i.e.* from point A at $\gamma = 0.0847$ to point B at $\gamma + d\gamma = 0.0848$. The blue dashed line indicates backward shear from point B at $\gamma + d\gamma = 0.0848$ to point C at $\gamma = 0.0847$. The magnitude of the potential energy difference is $|\Delta U(\gamma)| = |U_A - U_C|$ for $\gamma = 0.0847$.

$D(\gamma) = |\vec{R}(\gamma + d\gamma) - \vec{R}(\gamma)\boldsymbol{J}(\gamma)|/N$, where $\vec{R}(\gamma) = (\vec{r}_1, \vec{r}_2, \ldots, \vec{r}_N)$ gives the $3N$ particle coordinates at strain γ, $\boldsymbol{J}(\gamma) = \begin{bmatrix} e^{d\gamma} & 0 & 0 \\ 0 & e^{-d\gamma} & 0 \\ 0 & 0 & e^{d\epsilon} \end{bmatrix}$ is the affine transformation matrix describing pure shear in the x-y plane and com-

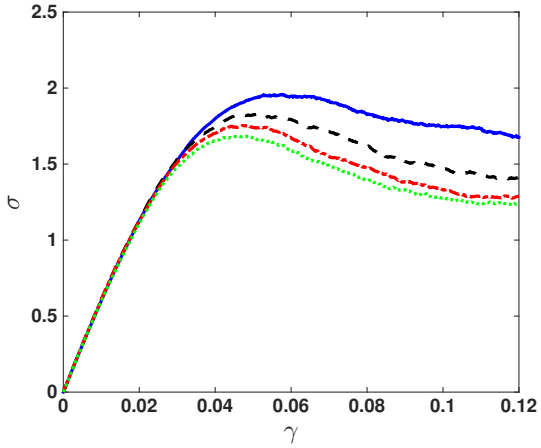

Figure 7: von Mises stress σ versus strain γ for zero-temperature glasses prepared at cooling rate $R_c = 10^{-3}$ and several system sizes: $N = 250$ (solid line), 500 (dashed line), 1000 (dash-dotted line), and 2000 (dotted line). The curves were averaged over 500 samples.

pression or expansion along the z-axis (depending on the sign of $d\epsilon = \ln[V(\gamma + d\gamma)/V(\gamma)]$) to maintain fixed pressure.

We show a scatter plot of $|\Delta U(\gamma)|$ versus $\mathcal{D}(\gamma)$ in Fig. 6 (b) for glasses prepared at $R_c = 10^{-5}$ and two system sizes $N = 250$ and 2000. We find a large gap in the values of the energy differences between "true" particle rearrangements ($|\Delta U| > U_t = 10^{-10}$) and "spurious" energy differences caused by numerical precision ($|\Delta U| < U_t$). In contrast, we find that true and spurious particle rearrangements (as identified via $|\Delta U|$) share a continuous range of values for the nonaffine displacements ($10^{-3} < \mathcal{D}(\gamma) < 10^{-2}$), which makes it difficult to set a non-arbitrary cutoff for defining particle rearrangements using $\mathcal{D}(\gamma)$. For $|\Delta U| > U_t$, we find that the energy differences grow with increasing non-affine displacement $\mathcal{D}(\gamma)$.

Appendix C: von Mises stress

In Fig. 1, we show the von Mises stress versus strain during the athermal, quasistatic pure shear deformation of binary Lennard-Jones glasses. The 3×3 stress tensor is given by

$$\Sigma_{\lambda\delta} = \frac{1}{V} \sum_{i>j} f_{ij\lambda} r_{ij\delta}, \tag{C1}$$

where $f_{ij\lambda}$ is the $\lambda = x, y, z$ component of the pairwise force $\vec{f}_{ij}$ that particle j exerts on particle i, and $r_{ij\delta}$ is the $\delta = x, y, z$ component of the center-to-center distance vector $\vec{r}_{ij}$ between particles i and j. The von Mises equivalent stress σ is given by the second invariant of the

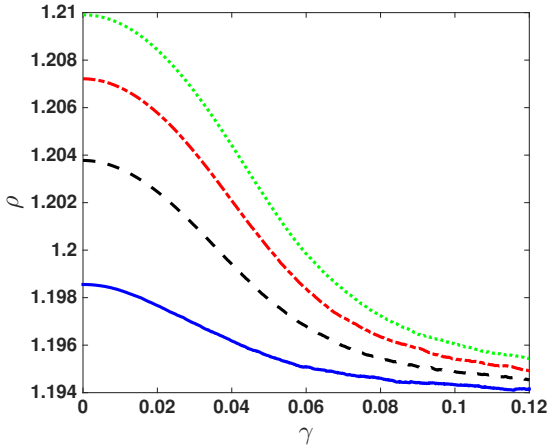

Figure 8: Reduced number density $\rho = N\sigma_{AA}^3/V$ of binary Lennard-Jones glasses containing $N = 2000$ particles prepared using cooling rates $R_c = 10^{-2}$ (solid curve), $R_c = 10^{-3}$ (dashed curve), $R_c = 10^{-4}$ (dash-dotted curve) and $R_c = 10^{-5}$ (dotted curve). These systems undergo athermal quasistatic pure shear at constant pressure $P = 10^{-8}$ as a function of strain γ. Each curve is averaged over 500 independent samples.

stress tensor:

$$\sigma = \sqrt{\frac{3}{2} Tr(\mathbf{\Sigma} + P\boldsymbol{I})^2}, \tag{C2}$$

where $\boldsymbol{I}$ is the identity tensor and $P = -1/3Tr(\mathbf{\Sigma})$ is the pressure [2]. We remove the residual stress $\sigma(0)$ from $\sigma(\gamma)$ so that the stress-strain curves are initialized to zero at $\gamma = 0$. In Fig. 7, we show the variation of stress versus strain ($\sigma(\gamma)$) with system size from $N = 250$ to 2000. For large $N > 1000$, $\sigma(\gamma)$ is nearly independent of system size.

Appendix D: Number density as a function of strain and cooling rate

The cooling rate dependence of the particle rearrangement statistics in our study is consistent with the fact that more slowly cooled glasses are more densely packed (and possess lower potential energy) than rapidly cooled glasses. In Fig. 8, we confirm that the density increases with decreasing cooling rate. In addition, the packing density decreases with strain for all cooling rates. In general, amorphous binary Lennard-Jones glasses with higher packing densities possess lower total potential energy since more pair interactions can be accommodated in the minimum of the pair potential.

[1] M. L. Falk and J. S. Langer, Physical Review E **57**, 7192 (1998).
[2] M. Utz, P. G. Debenedetti, and F. H. Stillinger, Physical Review Letters **84**, 1471 (2000).
[3] C. Maloney and A. Lemaître, Physical Review Letters **93**, 016001 (2004).
[4] B. A. Sun, H. B. Yu, W. Jiao, H. Y. Bai, D. Q. Zhao, and W. H. Wang, Physical Review Letters **105**, 35501 (2010).
[5] F. Spaepen, Acta Metallurgica **25**, 407 (1977).
[6] P. Schall, D. A. Weitz, and F. Spaepen, Science **318**, 1895 (2007).
[7] J. Ju, D. Jang, A. Nwankpa, and M. Atzmon, Journal of Applied Physics **109**, 053522 (2011).
[8] J. Ding, S. Patinet, M. L. Falk, Y. Cheng, and E. Ma, Proceedings of the National Academy of Sciences **111**, 14052 (2014).
[9] K. E. Jensen, D. A. Weitz, and F. Spaepen, Physical Review E **90**, 042305 (2014).
[10] M. Atzmon and J. D. Ju, Phys. Rev. E **90**, 042313 (2014).
[11] J. Ju and M. Atzmon, Journal of Alloys and Compounds **643**, S8 (2015).
[12] W. Chen, Z. Liu, J. Ketkaew, R. M. O. Mota, S.-H. Kim, M. Power, W. Samela, and J. Schroers, Acta Materialia **107**, 220 (2016).
[13] J. Antonaglia, X. Xie, G. Schwarz, M. Wraith, J. Qiao, Y. Zhang, P. K. Liaw, J. T. Uhl, and K. A. Dahmen, Scientific Reports **4**, 4382 (2014).
[14] G. Kumar, P. Neibecker, Y. H. Liu, and J. Schroers, Nature Communications **4**, 1536 (2013).
[15] O. Gendelman, P. K. Jaiswal, I. Procaccia, B. S. Gupta, and J. Zylberg, Europhysics Letters **109**, 16002 (2015).
[16] K.-W. Park, C.-M. Lee, M. Wakeda, Y. Shibutani, M. L. Falk, and J.-C. Lee, Acta Materialia **56**, 5440 (2008).
[17] I. Regev, J. Weber, C. Reichhardt, K. A. Dahmen, and T. Lookman, Nature Communications **6**, 8805 (2015).
[18] J. S. Harmon, M. D. Demetriou, W. L. Johnson, and K. Samwer, Physical Review Letters **99**, 135502 (2007).
[19] T. Fujita, Z. Wang, Y. Liu, H. Sheng, W. Wang, and M. Chen, Acta Materialia **60**, 3741 (2012).
[20] W. Dmowski, T. Iwashita, C.-P. Chuang, J. Almer, and T. Egami, Physical Review Letters **105**, 205502 (2010).
[21] J. Ding, Y. Cheng, and E. Ma, Applied Physics Letters **101**, 121917 (2012).
[22] A. Argon and H. Kuo, Materials Science and Engineering **39**, 101 (1979).
[23] J. S. Langer, Physical Review E **77**, 021502 (2008).
[24] M. L. Falk and J. S. Langer, Annual Review of Condensed Matter Physics **2**, 353 (2011).
[25] E. Bouchbinder, J. S. Langer, and I. Procaccia, Physical Review E **75**, 036107 (2007).
[26] D. L. Malandro and D. J. Lacks, The Journal of Chemical Physics **110**, 4593 (1999).
[27] F. H. Stillinger, Science **267**, 1935 (1995).
[28] P. G. Debenedetti and F. H. Stillinger, Nature **410**, 259 (2001).
[29] C. H. Rycroft and E. Bouchbinder, Physical review letters **109**, 194301 (2012).
[30] G. Kumar, S. Prades-Rodel, A. Blatter, and J. Schroers, Scripta Materialia **65**, 585 (2011).
[31] J. Zemp, M. Celino, B. Schönfeld, and J. F. Löffler, Physical Review Letters **115**, 165501 (2015).
[32] J. A., E. Bouchbinder, and I. Procaccia, Physical Review E **87**, 042310 (2013).
[33] D. J. Lacks and M. J. Osborne, Physical Review Letters **93**, 255501 (2004).
[34] C. E. Maloney and A. Lemaître, Physical Review E **74**, 016118 (2006).
[35] W. Kob and H. C. Andersen, Physical Review E **51**, 4626 (1995).
[36] M. P. Allen and D. J. Tildesley, *Computer simulation of liquids* (Oxford University Press, 1989).
[37] S. Plimpton, Journal of Computational Physics **117**, 1 (1995).
[38] M. E. Tuckerman, J. Alejandre, R. López-Rendón, A. L. Jochim, and G. J. Martyna, Journal of Physics A: Mathematical and General **39**, 5629 (2006).
[39] S. Büchner and A. Heuer, Physical Review E **60**, 6507 (1999).
[40] Y. Fan, T. Iwashita, and T. Egami, Physical Review Letters **115**, 045501 (2015).
[41] W. Li, H. Bei, Y. Tong, W. Dmowski, and Y. Gao, Applied Physics Letters **103**, 171910 (2013).
[42] C. Zhong, H. Zhang, Q. Cao, X. Wang, D. Zhang, U. Ramamurty, and J. Jiang, Scientific Reports **6** (2016).
[43] H. Sheng, W. Luo, F. Alamgir, J. Bai, and E. Ma, Nature **439**, 419 (2006).
[44] J. Lewandowski, W. Wang, and A. Greer, Philosophical Magazine Letters **85**, 77 (2005).
[45] H. B. Yu, X. Shen, Z. Wang, L. Gu, W. H. Wang, and H. Y. Bai, Physical Review Letters **108**, 015504 (2012).
[46] J. Schroers and W. L. Johnson, Physical Review Letters **93**, 255506 (2004).
[47] Y. Shi, J. Luo, F. Yuan, and L. Huang, Journal of Applied Physics **115**, 043528 (2014).
[48] A. Taub and F. Spaepen, Journal of Materials Science **16**, 3087 (1981).
[49] M. Kanik, P. Bordeenithikasem, G. Kumar, E. Kinser, and J. Schroers, Applied Physics Letters **105**, 131911 (2014).
[50] C. F. Schreck, R. S. Hoy, M. D. Shattuck, and C. S. OHern, Physical Review E **88**, 052205 (2013).
[51] I. Regev, T. Lookman, and C. Reichhardt, Physical Review E **88**, 062401 (2013).
[52] D. Fiocco, G. Foffi, and S. Sastry, Physical Review Letters **112**, 025702 (2014).
[53] N. V. Priezjev, Physical Review E **93**, 013001 (2016).
[54] T. Kawasaki and L. Berthier, Physical Review E **94**, 022615 (2016).
[55] H. G. E. Hentschel, P. K. Jaiswal, I. Procaccia, and S. Sastry, Physical Review E **92**, 062302 (2015).
[56] E. Lerner and I. Procaccia, Physical Review E **79**, 066109 (2009).
[57] S. Karmakar, E. Lerner, and I. Procaccia, Physical Review E **82**, 055103 (2010).